

Learning Probabilistic Structural Representation for Biomedical Image Segmentation

*Xiaoling Hu, Dimitris Samaras and Chao Chen

Stony Brook University

Abstract

Accurate segmentation of various fine-scale structures from biomedical images is a very important yet challenging problem. Existing methods use topological information as an additional training loss, but are ultimately learning a pixel-wise representation. In this paper, we propose the first deep learning method to learn a structural representation. We use discrete Morse theory and persistent homology to construct an one-parameter family of structures as the structural representation space. Furthermore, we learn a probabilistic model that can do inference tasks on such a structural representation space. We empirically demonstrate the strength of our method, i.e., generating true structures rather than pixel-maps with better topological integrity, and facilitating a human-in-the-loop annotation pipeline using the sampling of structures and structure-aware uncertainty.

1 Introduction

Segmentation of fine-scale structures such as vessels, neurons and membranes is an important task especial in biomedical applications [36, 13, 17]. Accurate delineation of these structures are crucial for downstream analysis and for understanding biomedical functionality. Classic segmentation algorithms [26, 16, 4–6] are prone to structural errors, e.g., broken connections, as they are mostly trained on pixel-wise losses such as cross-entropy. In recent years, new topology-relevant losses have been proposed to improve structural accuracy of deep segmentation networks [17, 18, 33, 28, 8]. These methods identify topologically critical locations at which the network is error-prone, and enforce the network to memorize these hard locations through increased loss weights. However, we argue that these loss-based methods are *only learning pixel-wise representations*, and thus will inevitably make structural errors, especially at the inference stage. See Fig. 1(c) for an illustration.

In order to fundamentally address the problem, we argue that it is essential to directly model and reason about the structures. In this paper, we propose the first deep neural network method that directly learns the structural representation of images. Given an input image properly denoised by a neural network, we adopt the classic (discrete) Morse theory [27, 15] to extract Morse complexes consisting of pieces of 0D, 1D and 2D structures. These Morse structures are singularities of the gradient field of the input function. Their combinations constitute a space of structures arising from the input function. See Fig. 2(c) for an illustration.

For further reasoning with structures, we propose to learn a probabilistic model over the structural space. The challenge is that the space consists of exponentially many branches and is thus of very high dimension. To reduce the learning burden, we introduce the theory of persistent homology [34, 9, 37] for structure pruning. Each branch has its own persistence measuring its relative saliency. By continuously thresholding the complete Morse complex in terms of persistence, we obtain a sequence

*Correspondence to: Xiaoling Hu <xiaolhu@cs.stonybrook.edu>.

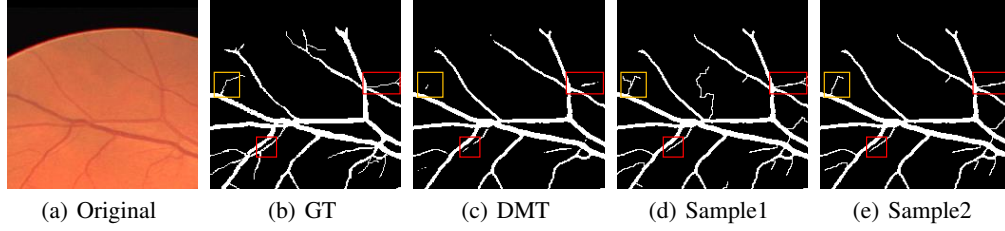


Figure 1: From left to right: **(a)** Original image, **(b)** Ground truth, **(c)** Segmentation map generated by standard DMT [18], **(d)** and **(e)** are two possible structure-preserving segmentation maps generated by our method. Compared with loss-function based segmentation methods, our method can generate both diverse and true structure-preserving segmentation maps. The red rectangles show structure-corrected regions by our method, and the yellow rectangle shows diversity region.

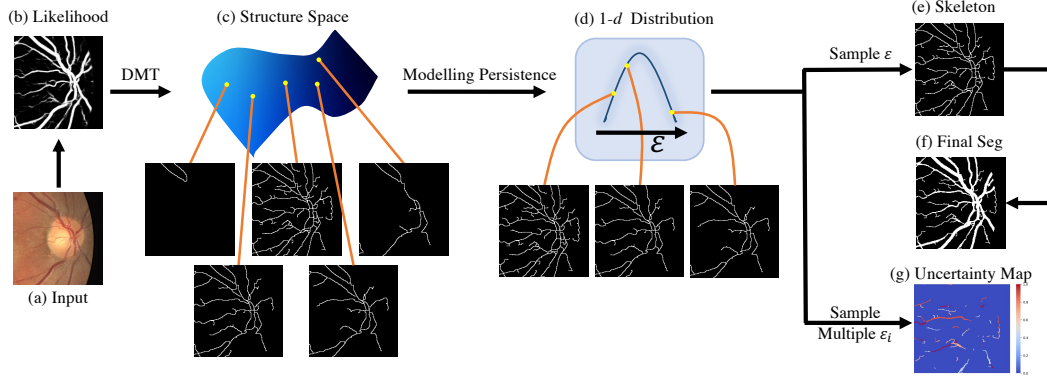


Figure 2: The probabilistic structural representation. **(a)** is a sample input, **(b)** is the predicted likelihood map, **(c)** is the whole structural space obtained by running discrete Morse theory algorithm on the likelihood map, **(d)** the 1- d structural family parametrized by the persistence threshold ϵ , as well as a Gaussian distribution over ϵ , **(e)** a sampled skeleton, **(f)** the final segmentation map generated using the skeleton sample, and **(g)** the uncertainty map generated by multiple segmentations.

of Morse complexes parameterized by the persistence threshold, ϵ . See Fig. 2(d). By learning a Gaussian over ϵ , we learn a parametric probabilistic model over these structures.

This parametric probabilistic model over structural space allows us to make direct structural predictions via sampling (Fig. 2(e)), and to estimate structure-wise uncertainty via sampling (Fig. 2(g)). The benefit is two-fold: First, direct prediction of structures will ensure the model outputs always have structural integrity, even at the inference stage. This is illustrated in Fig. 1(d) and (e). Samples from the probabilistic model are all feasible structural hypothesis based on the input image, with certain variations at uncertain locations. This is in contrast to state-of-the-art methods using pixel-wise representations (Fig. 1(c)). Note the original output structure (Fig. 2(e), also called skeleton) is only 1-pixel wide and may not serve as a good segmentation output. In the inference stage, we use a postprocessing step to grow the structures without changing topology as the final segmentation prediction (Fig. 2(f)). More details are provided in Sec. 3.2 and Fig. 5.

Second, the probabilistic structural model can be seamlessly incorporated into human-in-the-loop annotation workflows to facilitate large scale annotation of these complex structures. This is especially important in the biomedical domain where fine-scale structures are notoriously difficult to annotate, due to the complex 2D/3D morphology and low contrast near extremely thin structures. Our probabilistic model makes it possible to identify uncertain structures for efficient human quality control. Note that the structural space is crucial for uncertainty reasoning. As shown in Fig. 2(g), our proposed model uncertainty is only focusing on structures, whereas traditional pixel-wise uncertainty estimations [21] are much less informative without structural representation.

The main contributions of this paper are:

1. We propose the first deep segmentation network that learns a structural representation, based on discrete Morse theory and persistent homology.

2. We learn a probabilistic model over the structural space, which facilitates different tasks such as segmentation and uncertainty estimation.
3. We validate our method on various biomedical datasets with *rich and complex structures*. It outperforms state-of-the-art methods in both deterministic and probabilistic categories.

2 Related Work

Structure/Topology-aware deep image segmentation. A number of recent works have tried to segment with correct topology with additional topology-aware losses [28, 17, 8, 18, 33], which are close to the problem we are trying to address in this paper. Specifically, UNet-VGG [28] detects linear structures with pretrained filters, and cDice [33] introduces additional Dice loss for extracted skeleton structures. Another Topoloss [17, 8] learns to segment with correct topology explicitly with a differentiable loss by leveraging the concept of persistent homology. Similarly, DMT-loss [18] tries to identify the topological critical structures via discrete Morse theory.

All these methods propose additional topology-aware losses which are minimized if the topology of the segmented map is perfect. Though in the training stage, the models may fit the training set very well in terms of the topology and the topology-aware losses are minimized, it’s difficult for the models to reason the correct topology during the inference stage as the models are essentially topology agnostic. Topological priors have also been combined with encoder-decoder deep networks for semantic segmentation of microscopic neuroanatomical data [3]. Additionally, discrete Morse theory has been used for image analysis [9, 30, 37, 10], but only as a preprocessing step.

Different from all these loss functions based segmentation methods, our method, however, make structural predictions directly by using discrete Morse theory and persistent homology.

Segmentation uncertainty. Instead of traditional deterministic models with single prediction, a set of works have tried to generate multiple segmentations and explore the uncertainty in image segmentation tasks [21, 24] By using dropout, some methods [21, 22] learn a probability distribution instead of a single deterministic number for pixel classification. Though these methods are able to measure the pixel-level uncertainty, they are possible to generate inconsistent outputs as the probability for each pixel is estimated independently.

A possible way to obtain consistent outputs is by ensembling the results of different models [25]. However, as the composed models are trained separately, the final ensemble outputs are usually not diverse enough. Another solution is to train a common network with M heads [32, 19]. Though comparing to deep ensemble approaches, multi-head methods have the ability to generate diverse results, the major issue with both ensembling and multi-head models is that they are not scalable, and both of them require a fixed number of models/branches during the training stage. To overcome the scalability issue, Probabilistic-UNet [24] learns a distribution over the segmentation map given an input, and it is able to generate infinite number of possible outputs efficiently. We basically follow the logic of Probabilistic-UNet to design our probabilistic model, while we are targeting a quite different task: *how to generate diverse plausible structure-preserving segmentation maps given an image with rich structures?* As far as we know, none of existing works have tried to explore the structure-level uncertainty. Underlying the probabilistic model is the classical discrete Morse theory, which is used to construct the structural space from noisy likelihood maps.

3 Method

Our method starts by taking an input image, processing it with a neural network to obtain a reasonable likelihood map, and then using discrete Morse theory to construct a space of structures. These structures are the hypothesis structures one can infer from the input image. Next, we use persistent-homology-based thresholding to filter these structures, getting a linear size family of structures, parameterized by a threshold ϵ . We learn a 1D Gaussian distribution for the ϵ as our probabilistic model. Details will be provided below in Sec. 3.1. In Sec. 3.2, we will provide details on how our deep neural network is constructed, as illustrated in Fig. 4.

3.1 Constructing the Structural Space

In this section, we focus on how to construct a structural representation space using discrete Morse theory. We will then discuss how to prune the structural space using persistent homology. The resulting structural representation space will be used to build a probabilistic model.

Given a reasonably clean input (e.g., the likelihood map of a deep neural network, Fig. 2(b)), we treat the function as a terrain function, and the Morse theory [27] can help to capture the structures regardless of weak/blur conditions (Fig. 3). The weak part of a line in the continuous map can be viewed as the local dip in the mountain ridge of the terrain (see Fig. 3 as an illustration). In the language of Morse theory, the lowest point of this dip is a saddle point (S in Fig. 3(b)), and the mountain ridges which are connected to the saddle point (M_1S and M_2S) compose the stable manifold of the saddle point.

We mainly focus on 2D images in this paper, although extending to 3D images is natural. We consider two dimensional continuous function $f : \mathbb{R}^2 \rightarrow \mathbb{R}$. For a point $x \in \mathbb{R}^2$, the gradient can be computed as $\nabla f(x) = [\frac{\partial f}{\partial x_1}, \frac{\partial f}{\partial x_2}]^T$. We call a point $x = (x_1, x_2)$ *critical* if $\nabla f(x) = 0$. For a Morse function defined on \mathbb{R}^2 , a critical point could be a minimum, a saddle or a maximum.

Consider a continuous line (the red rectangle region in Fig. 3(a)) in a 2D likelihood map. Imagine if we put a ball on one point of the line, then $-\nabla f(x)$ indicates the direction which the ball will flow down. By definition, the ball will eventually flow to the critical points where $\nabla f(x) = 0$. The collection of points whose ball eventually flows to p ($\nabla f(p) = 0$) is defined as the stable manifold (denoted as $S(p)$) of point p . Intuitively, for a 2D function f , the stable manifold $S(p)$ of a minimum p is the entire valley of p (similar to watershed algorithm); similarly, the stable manifold $S(q)$ of a saddle point q consists of the whole ridge line which connecting two local maxima and goes through the saddle point. See Fig. 3(b) as an illustration.

For vessel data, the stable manifold of a saddle point contains the topological structures (line-like) of the continuous likelihood map predicted by deep neural networks, and they are exactly what we want to recover from noisy images. In practice, we adopt the discrete version of Morse theory for cubic data (images).

Discrete Morse theory. Take 2D image as a 2-dimensional cubical complex. A 2-dimensional cubical complex then contains 0-, 1-, and 2-dimensional cells, which correspond to vertices (pixels), edges and squares, respectively. In the setting of discrete Morse theory (DMT) [14, 15], a pair of adjacent cells, termed as discrete gradient vectors, compose gradient vector. Critical points ($\nabla f(x) = 0$) are those critical cells which are not in any discrete gradient vectors. In 2D domain, a minimum, a saddle and a maximum correspond to a critical vertex, a critical edge and a critical square respectively. A 1-stable manifold (the stable manifold of a saddle point) in 2D corresponds to a *V-path*, i.e., connecting two local maxima and a saddle. See Fig. 3(b).

In this way, by using discrete Morse theory, for a likelihood map from the deep neural network, we can extract all the stable manifolds of saddles, whose compositions constitute the whole structural space.

Formally, we call any combinations of these stable manifolds a structure. Fig. 2(c) illustrates 5 different structures. This structural space, however, is of exponential size. Assume N pieces of stable manifolds/branches (we also call these stable manifolds as branches for convenience). Any combinations of these stable manifolds/branches will be a potential structure. We will have 2^N possible structures. This can be computational prohibitive to construct and to model. We need a principled way to prune structures so the structural representation space has a controllable size.

Persistent homology for structural pruning. We propose to use the theory of persistent homology [34, 9, 37] to prune the structural space. Persistent homology is an important tool for topological data analysis [11, 12]. Intuitively, we grow a Morse complex by gradually including more and more discrete elements (called cells) from empty. A branch of the Morse complex is a special type of cell. Other types include vertices, patches, etc. Cells will be continuously added to the complex. New branches will born and existing branches will die. The persistence algorithm [12] pairs up all these critical cells as birth and death pairs. The difference of their function values is essentially the life time of the specific topological structure, which is called the *persistence*. The importance of a branch

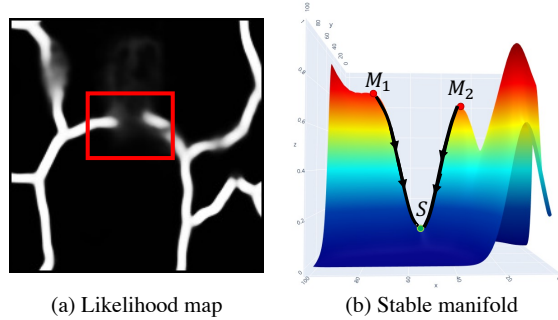


Figure 3: (a) shows a sample likelihood map from the deep neural network, and (b) is the terrain view of the red patch in (a) and illustrates the stable manifold of a saddle point in 2D case for a line-like structure.

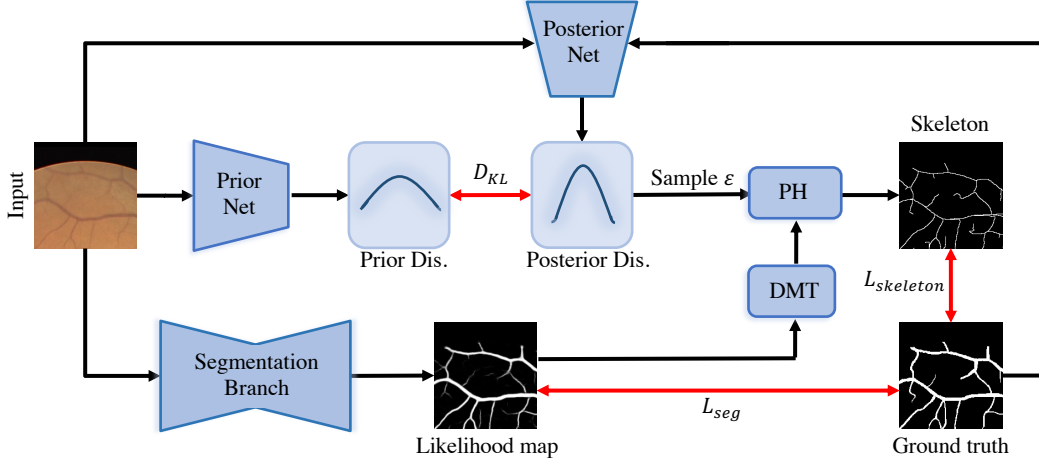


Figure 4: The overall workflow of the training stage. The red arrows indicate supervision.

is associated with its persistence. Intuitively, the longer the persistence of a specific branch is, the more important the branch is.

Recall our original construction of the structural space considers all possible combination of branches, and thus can have exponentially many combinations. Instead, we propose to only select branches with high persistence as important ones. By doing this, we will be able to prune the less important/noisy branches very efficiently, and recover the branches with true signals. Specifically, the structure pruning is done via the *Morse cancellation* (more details are included in Supplementary Material) operation. The persistence thresholding provides us the opportunity to obtain a linear-size of structural space. We start with the complete Morse complex, continuously grow the threshold ϵ . At each threshold, we obtain a structure by filtering with ϵ and only keeping the branches whose persistence is above ϵ . This gives a sequence of structures parametrized by ϵ . As shown in Fig. 2(d), the family of structures represent different structural densities.

The one-parameter space allows us to easily learn a probabilistic model and carry out various inference tasks such as segmentation, sampling, and uncertainty estimation. Specifically, we will learn a Gaussian distribution over the persistence threshold ϵ , $\epsilon \sim N(\mu, \sigma)$. More details will be provided in Sec. 3.2.

Approximation of Morse structures for volume data. Finally, we provide some additional technical details on construction of Morse complexes. In 2D setting, the stable manifold of saddles compose the line-like structures, and the captured Morse structures will essentially contain the *non-boundary edges*, which fits well with the vessel data. However, the output structures should always be *boundary edges* for volume data, which can't be dealt with the original discrete Morse theory. Consequently, we approximate the Morse structures of 2D volume data with the boundaries of the stable manifolds of local minima. As mentioned above, the stable manifold of a local minimum p in 2D setting corresponds the whole valley, and the boundaries of these valleys construct the approximation of the Morse structures for volume data. Similar to the original discrete Morse theory, we also introduce a persistence threshold parameter ϵ and use persistent homology to prune the less important branches. The details of the proposed persistent-homology filtered topology watershed algorithm are illustrated in Supplementary Material.

3.2 Neural Network Architecture

In this section, we introduce our neural network that learns the probabilistic model over structural representation. See Fig. 4 for an illustration of the overall pipeline.

Since the structural reasoning needs a sufficiently clean input function to construct discrete Morse complexes, our method first obtain such a likelihood map by training a segmentation branch which is supervised by the standard segmentation loss, cross-entropy loss, formally, $L_{seg} = L_{bce}(Y, S(X; \omega_{seg}))$, in which $S(X; \omega_{seg})$ is the output likelihood map, ω_{seg} is the segmentation branch's weight.

The output likelihood map, $S(X; \omega_{seg})$, is used as the input for the discrete Morse theory algorithm (DMT), which generates a discrete Morse complex consisting of all possible Morse branches from the likelihood map. Thresholding these branches using persistent homology with different ϵ 's will produce different structures. We refer to the DMT computation and the persistent homology thresholding operation as f_{DMT} and f_{PH} . So given a likelihood map $S(X; \omega_{seg})$ and a threshold ϵ , we can generate a structure (which we call a skeleton):

$$S_{skeleton}(\epsilon) = f_{PH}(f_{DMT}(S(X; \omega_{seg})); \epsilon) \quad (1)$$

Next, we discuss how to learn the probabilistic model. Recall we want to learn a Gaussian distribution over the persistent homology threshold, $\epsilon \sim N(\mu, \sigma)$. The parameters μ and σ are learned by a neural network called the *posterior network*. The network uses the input image X and the corresponding ground truth mask Y as input, and outputs the parameters $\mu(X, Y; \omega_{post})$ and $\sigma(X, Y; \omega_{post})$. ω_{post} is the parameter of the network.

During training, at each iteration, we draw a sample ϵ from the distribution ($\epsilon \sim N(\mu, \sigma)$). Using the sample ϵ , together with the likelihood map, we can generate the corresponding sample structure, $S_{skeleton}(\epsilon)$. This skeleton will be compared with the ground truth for supervision. To compare a sampled skeleton, $S_{skeleton}(\epsilon)$, with ground truth Y , we use the skeleton to mask both Y and the likelihood map $S(X; \omega_{seg})$, and then compare the skeleton-masked ground truth and the likelihood using cross-entropy loss: $L_{bce}(Y \circ S_{skeleton}(\epsilon), S(X; \omega_{seg}) \circ S_{skeleton}(\epsilon))$.

To learn the distribution, we use the expected loss:

$$L_{skeleton} = \mathbb{E}_{\epsilon \sim N(\mu, \sigma)} L_{bce}(Y \circ S_{skeleton}(\epsilon), S(X; \omega_{seg}) \circ S_{skeleton}(\epsilon)) \quad (2)$$

The loss can be backpropagated through the posterior network through reparameterization technique [23]. More details will be provided in Supplemental. Note that this loss will also provide supervision to the segmentation network through the likelihood map.

Learning a prior network from the posterior network. Although our posterior network can learn the distribution well, it rely on the ground truth mask Y as input. This is not available at inference stage. To address this issue, inspired by Probabilistic-UNet [24], we use another network to learn the distribution of ϵ with only the image X as input. We call this network the *prior net*. We denote by P the distribution using parameters predicted by the prior network, and denote by Q the distribution predicted by the posterior network.

During the training, we want to use the prior net to mimic the posterior net; and then in the inference stage, we can use the prior net to obtain a reliable distribution over ϵ with only the image X . Thus, we incorporate the Kullback-Leibler divergence of these two distributions,

$$D_{KL}(Q||P) = \mathbb{E}_{\epsilon \sim Q}(\log \frac{Q}{P}) \quad (3)$$

which measures the differences of prior distribution $P(N(\mu_{prior}, \sigma_{prior}))$ and the posterior distribution $Q(N(\mu_{post}, \sigma_{post}))$.

Training the neural network. The final loss is composed by the standard segmentation loss, the skeleton loss $L_{skeleton}$, and the KL divergence loss, with two hyperparameters α and β to balance the three terms,

$$L(X, Y) = L_{seg} + \alpha L_{skeleton} + \beta D_{KL}(Q||P) \quad (4)$$

The network is trained to jointly optimize the segmentation branch and the probabilistic branch (containing both prior and posterior nets) simultaneously. During the training stage, the KL divergence loss (D_{KL}) pushes the prior distribution towards the posterior distribution. The training scheme is also illustrated in Fig. 4.

Inference stage: generating structure-preserving segmentation maps. In the inference stage, given an input image, we are able to produce unlimited number of plausible structure-preserving skeletons via sampling. We use a postprocessing step to grow the 1-pixel wide structures/skeletons without changing its topology as the final segmentation prediction. Specifically, the skeletons are overlaid on the binarized initial segmentation map (Fig. 5(c)), and only the connected components which exist in the skeletons are kept as the final segmentation maps. In this way, each plausible skeleton generates one final segmentation map and it has exact the same topology as the corresponding skeleton. The pipeline of the procedure is illustrated in Fig. 5.

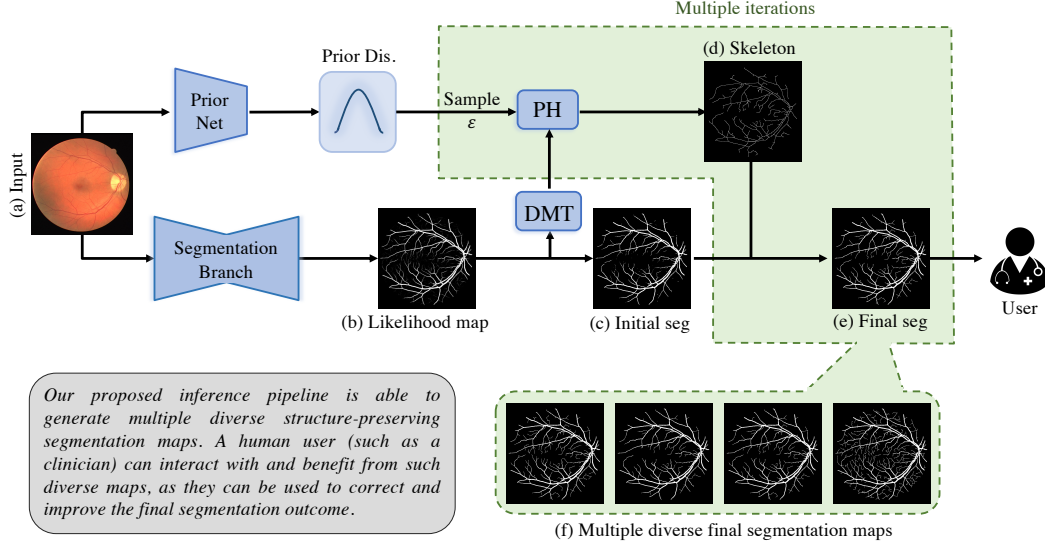


Figure 5: The inference and human-in-the-loop pipeline.

4 Experiments

Datasets. We use three datasets to validate the efficacy of the proposed method: **ISBI13** [1] (volume), **CREMI** (volume), and **DRIVE** [35] (vessel). More details are included in Supplementary Material.

Evaluation metrics. We use four different evaluation metrics: **Dice score**, **ARI**, **VOI**, and **Betti number error**. Dice is a popular pixel-wise segmentation metric, and the other three are structure/topology-aware segmentation metrics. More details are included in Supplementary Material.

Baselines. We compare the proposed method with two kinds of baselines: 1) Standard segmentation baselines: **DIVE** [13], **UNet** [31], **UNet-VGG** [28], **TopoLoss** [17] and **DMT** [18]. 2) Probabilistic-based segmentation methods: **Dropout UNet** [21] and **Probabilistic-UNet** [24]. More details about these baselines are included in Supplementary Material.

Illustration of generating final structure-preserving segmentation maps and human-in-the-loop annotation workflow. In the inference stage, we are able to generate a continuous likelihood map (Fig. 5(b)) and a set of structure-preserving skeletons (Fig. 5(d)) simultaneously for a given image. By growing the structure-preserving skeleton, we will finally generate the *true structure-preserving* segmentation map (Fig. 5(e)). Note that Fig. 5(d) and Fig. 5(e) have exact the same topology, which both improve a lot compared with initial segmentation (Fig. 5(c)) in terms of topology/structure.

The proposed method can also be used as an image annotation workflow for biomedical images with rich structures. As mentioned in the motivation section and illustrated in Fig. 1(c), the binary mask generated by standard segmentation methods may still have topological errors and noise, which can not be directly used in practice. With the proposed method, given an image (Fig. 5(a)), the users can conduct the inference a few times (such as 10) and be able to generate a set of structure-preserving segmentation masks (Fig. 5(f)). By choosing the one which looks most reasonable, human-in-the-loop can then start from a good point. By removing the unnecessary structures and redrawing the missing structures, we can efficiently annotate one image with rich structures. The whole inference pipeline and human-in-the-loop structure-aware image annotation workflow is illustrated in Fig. 5.

Quantitative and qualitative results. Table 1 shows the quantitative results comparing to several baselines. Note that for deterministic methods, the numbers are computed directly based on the outputs; while for probabilistic methods, we generate five segmentation masks and report the averaged numbers over the five segmentation masks for each image (for both the baselines and the proposed method). We use t-test to determine the statistical significance and highlight the significant better results. From the table, we can observe that the proposed method achieves significant better performances in terms of topology-aware metrics (ARI, VOI and Betti Error).

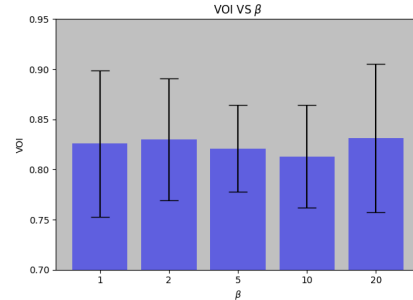
Table 1: Quantitative results for different models on three different biomedical datasets.

Method	Dice \uparrow	ARI \uparrow	VOI \downarrow	Betti Error \downarrow
ISBI13 (Volume)				
DIVE [13]	0.9658 ± 0.0020	0.6923 ± 0.0134	2.790 ± 0.025	3.875 ± 0.326
UNet [31]	0.9649 ± 0.0057	0.7031 ± 0.0256	2.583 ± 0.078	3.463 ± 0.435
UNet-VGG [28]	0.9623 ± 0.0047	0.7483 ± 0.0367	1.534 ± 0.063	2.952 ± 0.379
TopoLoss [17]	0.9689 ± 0.0026	0.8064 ± 0.0112	1.436 ± 0.008	1.253 ± 0.172
DMT [18]	0.9712 ± 0.0047	0.8289 ± 0.0189	1.176 ± 0.052	1.102 ± 0.203
Dropout UNet [21]	0.9591 ± 0.0031	0.7127 ± 0.0181	2.483 ± 0.046	3.189 ± 0.371
Prob.-UNet [24]	0.9618 ± 0.0019	0.7091 ± 0.0201	2.319 ± 0.041	3.019 ± 0.233
Ours	0.9637 ± 0.0032	0.8417 ± 0.0114	1.013 ± 0.081	0.972 ± 0.141
CREMI (Volume)				
DIVE [13]	0.9542 ± 0.0037	0.6532 ± 0.0247	2.513 ± 0.047	4.378 ± 0.152
UNet [31]	0.9523 ± 0.0049	0.6723 ± 0.0312	2.346 ± 0.105	3.016 ± 0.253
UNet-VGG [28]	0.9489 ± 0.0053	0.7853 ± 0.0281	1.623 ± 0.083	1.973 ± 0.310
TopoLoss [17]	0.9596 ± 0.0029	0.8083 ± 0.0104	1.462 ± 0.028	1.113 ± 0.224
DMT [18]	0.9653 ± 0.0019	0.8203 ± 0.0147	1.089 ± 0.061	0.982 ± 0.179
Dropout UNet [21]	0.9518 ± 0.0018	0.6814 ± 0.0202	2.195 ± 0.087	3.190 ± 0.198
Prob.-UNet [24]	0.9531 ± 0.0022	0.6961 ± 0.0115	1.901 ± 0.107	2.931 ± 0.177
Ours	0.9541 ± 0.0031	0.8509 ± 0.0054	0.918 ± 0.074	0.906 ± 0.085
DRIVE (Vessel)				
DIVE [13]	0.7543 ± 0.0008	0.8407 ± 0.0257	1.936 ± 0.127	3.276 ± 0.642
UNet [31]	0.7491 ± 0.0027	0.8343 ± 0.0413	1.975 ± 0.046	3.643 ± 0.536
UNet-VGG [28]	0.7218 ± 0.0013	0.8870 ± 0.0386	1.167 ± 0.026	2.784 ± 0.293
TopoLoss [17]	0.7621 ± 0.0036	0.9024 ± 0.0113	1.083 ± 0.006	1.076 ± 0.265
DMT [18]	0.7733 ± 0.0039	0.9077 ± 0.0021	0.876 ± 0.038	0.873 ± 0.402
Dropout UNet [21]	0.7410 ± 0.0019	0.8331 ± 0.0152	2.013 ± 0.072	3.121 ± 0.334
Prob.-UNet [24]	0.7429 ± 0.0020	0.8401 ± 0.1881	1.873 ± 0.081	3.080 ± 0.206
Ours	0.7545 ± 0.0043	0.9141 ± 0.0036	0.813 ± 0.051	0.735 ± 0.104

Fig. 6 shows qualitative results. Comparing with DMT [18], our method is able to produce a set of true structure-preserving segmentation maps, as illustrated in Fig. 6(e-g). Note that compared with the existing topology-aware segmentation methods, our method is more capable of recovering the weak connections by using Morse skeletons as hints. More qualitative results are included in Supplementary Material.

Ablation study of loss weights. We observe that the performances of our method are quite robust to the loss weights α and β . As the learned distribution over the persistence threshold might affect the final performances, we conduct an ablation study in terms of the weight of KL divergence loss (β) on DRIVE dataset. The results are reported in Fig. 7. When $\beta = 10$, the model achieves slightly better performance in terms of VOI (0.813 ± 0.051 , the smaller the better) than other choices. Note that, for all the experiments, we set $\alpha = 1$.

Illustration of the structure-level uncertainty. In this section, we’d like to explore the structure-level uncertainty based on the sampled segmentation masks. We show three sampled masks (Fig. 8(c-e)) in the inference stage for a given image (Fig. 8(a)), and the structure-wise uncertainty map (Fig. 8(f)). Note that uncertainty map is generated by taking variance across all the samples (the number is 10 for this specific case). Different from pixel-level uncertainty, each small branch has the same uncertainty value with our method. If we look at the original image, we will find that the uncertainties are usually caused by the weak signals (small branches) of the original image. The weak signals of the original image make the deep model difficult to predict these locations correctly and confidently, especially in structure wise. Actually this also makes sense in real cases. Different from natural images, even experts can not always reach a consensus for biomedical image annotation [2, 7]. It is beneficial that our model can both generate a set of plausible segmentation results and the uncertainty

Figure 7: Ablation study results for β .

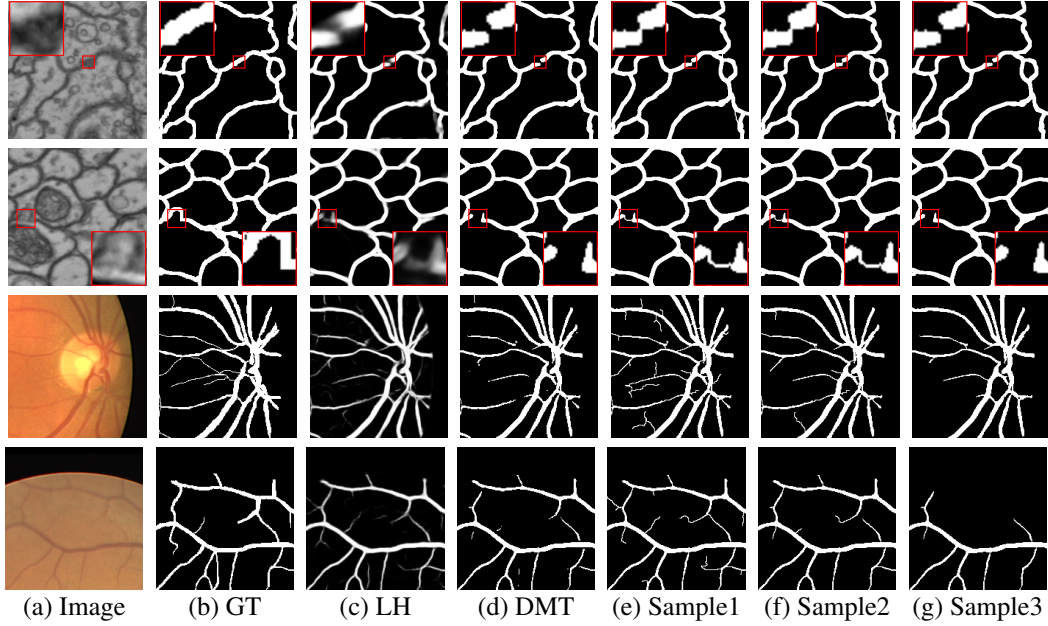


Figure 6: Qualitative results of the proposed method compared to DMT-loss [18]. From left to right: (a) sample image, (b) ground truth, (c) continuous likelihood map and (d) thresholded binary mask for DMT [18], and (e-g) three sampled segmentation maps generated by our method.

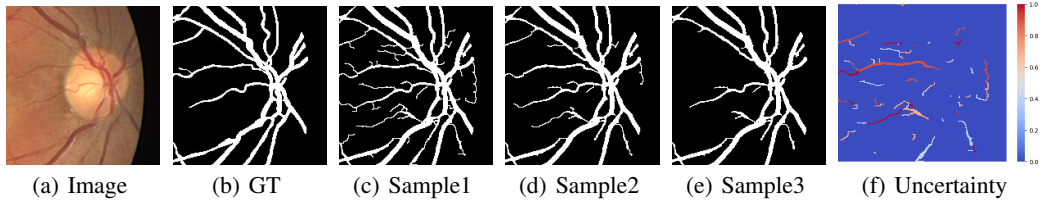


Figure 8: An illustration of structure-level uncertainty.

map as hints for further quality control. More explorations of structure-level uncertainty are included in Supplementary Material.

The advantage of the joint training and optimization. Another straightforward alternative of the proposed approach is to use the discrete Morse theory to postprocess the continuous likelihood map obtained from the standard segmentation networks. In this way, we can still obtain structure-clean segmentation maps, but there are two main issues: 1) if the segmentation network itself is structure-agnostic, we’ll not be able to generate satisfactory results even with the postprocessing, and 2) we have to manually choose the persistence threshold to prune the unnecessary branches for each image, which is annoying and unrealistic in practice. The proposed joint training strategy overcomes both these two issues. First, during the training, we incorporate the structure-aware loss ($L_{skeleton}$). Consequently, the trained segmentation branch itself is structure-aware essentially. On the other hand, with the prior and posterior nets, we are able to learn a reliable distribution of the persistence threshold (ϵ) given an image in the inference stage. Sampling over the distribution makes it possible to generate satisfactory structure-preserving segmentation maps within a few trials (the inference won’t take long), which is more much efficient.

5 Conclusion

Instead of learning pixel-wise representation, we propose to learn structural representation with a probabilistic model to segment with correct topology. Specifically, we construct the structural space by leveraging classical discrete Morse theory. And then we build a probabilistic model to learn a distribution over structures. The model is trained and optimized jointly. In the inference stage, we are able to generate a set of structure-preserving segmentation maps and explore the structure-level

uncertainty, which is beneficial for human-in-the-loop quality control. Extensive experiments have been conducted to demonstrate the efficacy of the proposed method.

Limitation. This paper is the first work to learn structural representation for image segmentation task. As a pioneer work of this specific task, though addressing the problem from a novel view, pruning the structures with a global threshold (the sampled persistence threshold ϵ) is somewhat brutal. Ideally, we should be able to adaptively prune the unnecessary branches locally, which is left for further work.

References

- [1] I Arganda-Carreras, HS Seung, A Vishwanathan, and D Berger. 3d segmentation of neurites in em images challenge-isbi 2013, 2013.
- [2] Samuel G Armato III, Geoffrey McLennan, Luc Bidaut, Michael F McNitt-Gray, Charles R Meyer, Anthony P Reeves, Binsheng Zhao, Denise R Aberle, Claudia I Henschke, Eric A Hoffman, et al. The lung image database consortium (lidc) and image database resource initiative (idri): a completed reference database of lung nodules on ct scans. *Medical physics*, 2011.
- [3] Samik Banerjee, Lucas Magee, Dingkan Wang, Xu Li, Bing-Xing Huo, Jaikishan Jayakumar, Katherine Matho, Meng-Kuan Lin, Keerthi Ram, Mohanasankar Sivaprakasam, et al. Semantic segmentation of microscopic neuroanatomical data by combining topological priors with encoder-decoder deep networks. *Nature Machine Intelligence*, 2020.
- [4] Liang-Chieh Chen, George Papandreou, Iasonas Kokkinos, Kevin Murphy, and Alan L Yuille. Semantic image segmentation with deep convolutional nets and fully connected crfs. *arXiv preprint arXiv:1412.7062*, 2014.
- [5] Liang-Chieh Chen, George Papandreou, Iasonas Kokkinos, Kevin Murphy, and Alan L Yuille. Deeplab: Semantic image segmentation with deep convolutional nets, atrous convolution, and fully connected crfs. *TPAMI*, 2018.
- [6] Liang-Chieh Chen, George Papandreou, Florian Schroff, and Hartwig Adam. Rethinking atrous convolution for semantic image segmentation. *arXiv preprint arXiv:1706.05587*, 2017.
- [7] Kenneth Clark, Bruce Vendt, Kirk Smith, John Freymann, Justin Kirby, Paul Koppel, Stephen Moore, Stanley Phillips, David Maffitt, Michael Pringle, et al. The cancer imaging archive (tcia): maintaining and operating a public information repository. *Journal of digital imaging*, 2013.
- [8] J Clough, N Byrne, I Oksuz, VA Zimmer, JA Schnabel, and A King. A topological loss function for deep-learning based image segmentation using persistent homology. *TPAMI*, 2020.
- [9] O. Delgado-Friedrichs, V. Robins, and A. Sheppard. Skeletonization and partitioning of digital images using discrete morse theory. *TPAMI*, 2015.
- [10] T. Dey, J. Wang, and Y. Wang. Road network reconstruction from satellite images with machine learning supported by topological methods. In *Proc. 27th ACM SIGSPATIAL Intl. Conf. Adv. Geographic Information Systems (GIS)*, 2019.
- [11] Herbert Edelsbrunner and John Harer. *Computational topology: an introduction*. American Mathematical Soc., 2010.
- [12] Herbert Edelsbrunner, David Letscher, and Afra Zomorodian. Topological persistence and simplification. In *FOCS*, 2000.
- [13] Ahmed Fakhry, Hanchuan Peng, and Shuiwang Ji. Deep models for brain em image segmentation: novel insights and improved performance. *Bioinformatics*, 2016.
- [14] R. Forman. Morse theory for cell complexes. *Advances in mathematics*, 1998.
- [15] Robin Forman. A user’s guide to discrete morse theory. *Sém. Lothar. Combin*, 2002.

- [16] Kaiming He, Georgia Gkioxari, Piotr Dollár, and Ross Girshick. Mask r-cnn. In *ICCV*, 2017.
- [17] Xiaoling Hu, Fuxin Li, Dimitris Samaras, and Chao Chen. Topology-preserving deep image segmentation. In *NeurIPS*, 2019.
- [18] Xiaoling Hu, Yusu Wang, Li Fuxin, Dimitris Samaras, and Chao Chen. Topology-aware segmentation using discrete morse theory. In *ICLR*, 2021.
- [19] Eddy Ilg, Ozgun Cicek, Silvio Galesso, Aaron Klein, Osama Makansi, Frank Hutter, and Thomas Brox. Uncertainty estimates and multi-hypotheses networks for optical flow. In *ECCV*, 2018.
- [20] Viren Jain, Benjamin Bollmann, Mark Richardson, Daniel R Berger, Moritz N Helmstaedter, Kevin L Briggman, Winfried Denk, Jared B Bowden, John M Mendenhall, Wickliffe C Abraham, et al. Boundary learning by optimization with topological constraints. In *CVPR*, 2010.
- [21] Alex Kendall, Vijay Badrinarayanan, and Roberto Cipolla. Bayesian segnet: Model uncertainty in deep convolutional encoder-decoder architectures for scene understanding. *arXiv preprint arXiv:1511.02680*, 2015.
- [22] Alex Kendall and Yarin Gal. What uncertainties do we need in bayesian deep learning for computer vision? In *NeurIPS*, 2017.
- [23] Diederik P Kingma and Max Welling. Auto-encoding variational bayes. *arXiv preprint arXiv:1312.6114*, 2013.
- [24] Simon Kohl, Bernardino Romera-Paredes, Clemens Meyer, Jeffrey De Fauw, Joseph R Ledsam, Klaus Maier-Hein, SM Eslami, Danilo Jimenez Rezende, and Olaf Ronneberger. A probabilistic u-net for segmentation of ambiguous images. In *NeurIPS*, 2018.
- [25] Balaji Lakshminarayanan, Alexander Pritzel, and Charles Blundell. Simple and scalable predictive uncertainty estimation using deep ensembles. In *NeurIPS*, 2017.
- [26] Jonathan Long, Evan Shelhamer, and Trevor Darrell. Fully convolutional networks for semantic segmentation. In *CVPR*, 2015.
- [27] John Milnor. *Morse theory.(AM-51)*, volume 51. Princeton university press, 1963.
- [28] Agata Mosinska, Pablo Marquez-Neila, Mateusz Koziński, and Pascal Fua. Beyond the pixel-wise loss for topology-aware delineation. In *CVPR*, 2018.
- [29] William M Rand. Objective criteria for the evaluation of clustering methods. *Journal of the American Statistical association*, 1971.
- [30] Vanessa Robins, Peter John Wood, and Adrian P Sheppard. Theory and algorithms for constructing discrete morse complexes from grayscale digital images. *TPAMI*, 2011.
- [31] Olaf Ronneberger, Philipp Fischer, and Thomas Brox. U-net: Convolutional networks for biomedical image segmentation. In *MICCAI*, 2015.
- [32] Christian Rupprecht, Iro Laina, Robert DiPietro, Maximilian Baust, Federico Tombari, Nassir Navab, and Gregory D Hager. Learning in an uncertain world: Representing ambiguity through multiple hypotheses. In *ICCV*, 2017.
- [33] Suprosanna Shit, Johannes C Paetzold, Anjany Sekuboyina, Ivan Ezhov, Alexander Unger, Andrey Zhylyka, Josien PW Pluim, Ulrich Bauer, and Bjoern H Menze. cldice-a novel topology-preserving loss function for tubular structure segmentation. In *CVPR*, 2021.
- [34] Thierry Sousbie. The persistent cosmic web and its filamentary structure–i. theory and implementation. *Monthly Notices of the Royal Astronomical Society*, 2011.
- [35] Joes Staal, Michael D Abràmoff, Meindert Niemeijer, Max A Viergever, and Bram Van Ginneken. Ridge-based vessel segmentation in color images of the retina. *TMI*, 2004.

- [36] Giles Tetteh, Velizar Efremov, Nils D Forkert, Matthias Schneider, Jan Kirschke, Bruno Weber, Claus Zimmer, Marie Piraud, and Björn H Menze. Deepvesselnet: Vessel segmentation, centerline prediction, and bifurcation detection in 3-d angiographic volumes. *Frontiers in Neuroscience*, 2020.
- [37] S. Wang, Y. Wang, and Y. Li. Efficient map reconstruction and augmentation via topological methods. In *Proc. 23rd ACM SIGSPATIAL*, 2015.

Checklist

1. For all authors...
 - (a) Do the main claims made in the abstract and introduction accurately reflect the paper’s contributions and scope? [\[Yes\]](#)
 - (b) Did you describe the limitations of your work? [\[Yes\]](#)
 - (c) Did you discuss any potential negative societal impacts of your work? [\[N/A\]](#)
 - (d) Have you read the ethics review guidelines and ensured that your paper conforms to them? [\[Yes\]](#)
2. If you are including theoretical results...
 - (a) Did you state the full set of assumptions of all theoretical results? [\[N/A\]](#)
 - (b) Did you include complete proofs of all theoretical results? [\[N/A\]](#)
3. If you ran experiments...
 - (a) Did you include the code, data, and instructions needed to reproduce the main experimental results (either in the supplemental material or as a URL)? [\[Yes\]](#) See the Supplemental Material.
 - (b) Did you specify all the training details (e.g., data splits, hyperparameters, how they were chosen)? [\[Yes\]](#) See Sec. 4 and the Supplemental Material.
 - (c) Did you report error bars (e.g., with respect to the random seed after running experiments multiple times)? [\[Yes\]](#) See Tab. 1.
 - (d) Did you include the total amount of compute and the type of resources used (e.g., type of GPUs, internal cluster, or cloud provider)? [\[Yes\]](#) See the Supplemental Material.
4. If you are using existing assets (e.g., code, data, models) or curating/releasing new assets...
 - (a) If your work uses existing assets, did you cite the creators? [\[Yes\]](#)
 - (b) Did you mention the license of the assets? [\[N/A\]](#)
 - (c) Did you include any new assets either in the supplemental material or as a URL? [\[Yes\]](#)
 - (d) Did you discuss whether and how consent was obtained from people whose data you’re using/curating? [\[N/A\]](#)
 - (e) Did you discuss whether the data you are using/curating contains personally identifiable information or offensive content? [\[N/A\]](#)
5. If you used crowdsourcing or conducted research with human subjects...
 - (a) Did you include the full text of instructions given to participants and screenshots, if applicable? [\[N/A\]](#)
 - (b) Did you describe any potential participant risks, with links to Institutional Review Board (IRB) approvals, if applicable? [\[N/A\]](#)
 - (c) Did you include the estimated hourly wage paid to participants and the total amount spent on participant compensation? [\[N/A\]](#)

A Appendix

Appendix B illustrates structure-level uncertainty compared with traditional pixel-level uncertainty.

Appendix C shows more qualitative results.

Appendix D provides the details of Morse cancellation.

Appendix E illustrates the details of persistent-homology filtered topology watershed algorithm.

Appendix F describes the reparameterization technique.

Appendix G provides the details of the datasets used in this paper.

Appendix H illustrates the details of the metrics used in this paper.

Appendix I describes the details of the baselines used in this paper.

Appendix J provides the computational resources for all the conducted experiments.

B Illustration of the structure-level uncertainty

Fig. 9 shows the comparison of traditional pixel-level uncertainty and the proposed structure-level uncertainty. Specifically, Fig. 9(c) is a sampled segmentation result by Prob.-UNet [24], and Fig. 9(d) is the pixel uncertainty map from Prob.-UNet [24]. Different from traditional pixel-level uncertainty, our proposed structure-level uncertainty (Fig. 9(h)) can focus on the structures.

We also overlay the structure-level uncertainty (Fig. 9(h)) on the original image (Fig. 9(a)), which is shown in Fig. 10. By comparison with the original image, we can observe that the structure-level uncertainty is mainly caused by the weak signals in the original image.

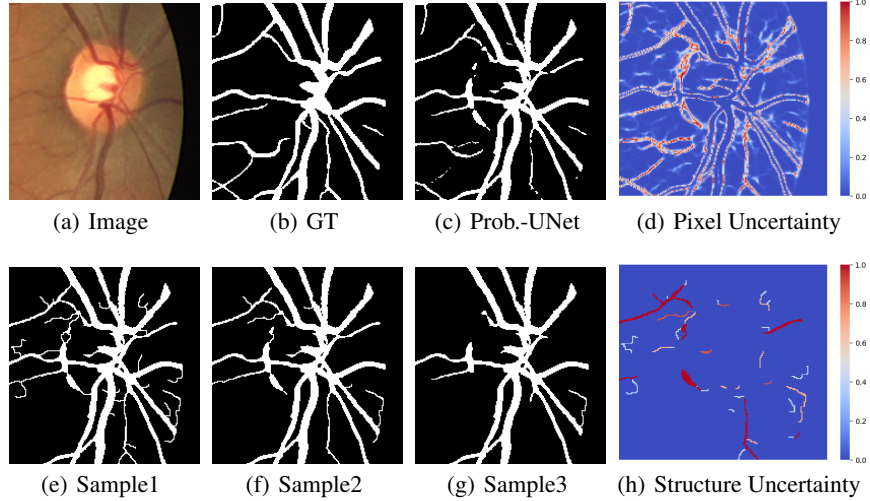


Figure 9: An illustration of structure-level uncertainty.

C Qualitative results

Fig. 11 shows more qualitative results. From Fig. 11, we can observe that the proposed method can generate both diverse and structure-preserving segmentation maps.

D Morse cancellation

As the predicted likelihood map is noisy, the extracted discrete gradient field $M(K)$ could also be noisy. Fortunately, the discrete Morse theory provides an elegant way to cancel critical simplice

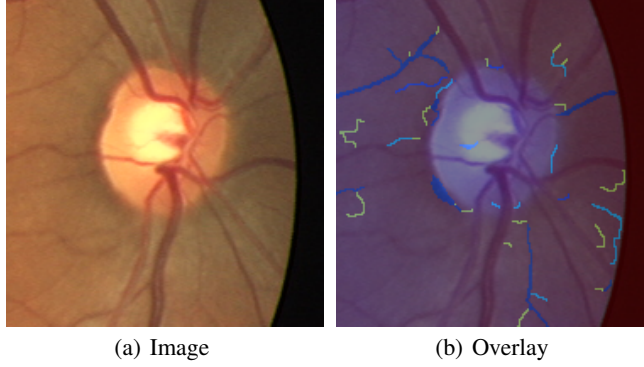


Figure 10: Overlay the structure-level uncertainty on the original image.

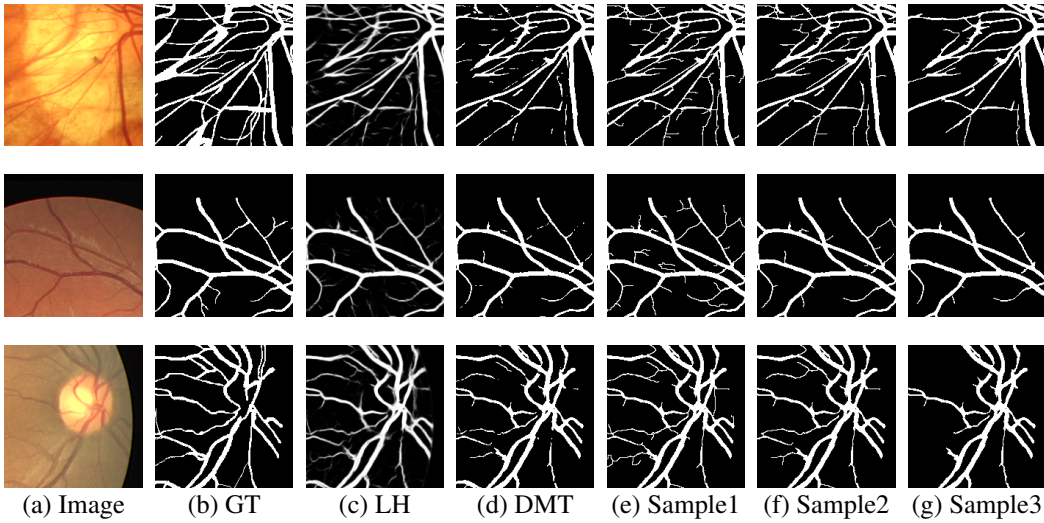


Figure 11: Qualitative results of the proposed method compared to DMT-loss [18]. From left to right: **(a)** sample image, **(b)** ground truth, **(c)** continuous likelihood map and **(d)** thresholded binary mask for DMT [18], and **(e-g)** three sampled segmentation maps generated by our method.

pairs and ignore the the unimportant Morse branches. Particularly, if there is a unique V-path $\pi = \delta = \delta_0, \gamma_1, \delta_1, \dots, \delta_s, \gamma_{s+1} = \gamma$ from δ to γ , then the pair of critical simplices $\langle \delta^{(p+1)}, \gamma^p \rangle$ is *cancellable*. By removing all V-pairs along these path, and adding (δ_{i-1}, γ_i) to $M(K)$ for any $i \in [1, s + 1]$, the *Morse cancellation operation* reverses all V-pairs along this path. In this way, neither δ nor γ is critical after the cancellation operation and we can prune/remove the corresponding stable manifold/branch. More details can be found in [18].

E Approximation for volume data

As illustrated in the main text, we propose a persistent-homology filtered topology watershed algorithm to obtain the approximation of Morse structures for volume data. The details are illustrated in Alg. 1.

F Reparameterization technique

We adopt the reparameterization technique of VAE to make the network differentiable and be able to backpropagate.

Algorithm 1: Persistent-Homology filtered Topology Watershed Algorithm

Input: a grid 2D image, and a threshold θ

Output: Morse structures for volume data

Definition: $G = (V, E)$ denote a graph; $f(v)$ is the intensity value of node v ; $\text{lower_star}(v) = \{(u, v) \in E | f(u) < f(v)\}$; $cc(v)$ is the connected component id of node v .

```
1:  $PD = \emptyset$ ; Build the proximity graph (4-connectivity) for 2D grid image;
2:  $U = V$  sorted according  $f(v)$ ;  $T$  a sub-graph, which includes all the nodes and edges whose
   value  $< t$ .
3: for  $v$  in  $U$  do
4:    $t = f(v)$ ,  $T = T + \{v\}$ 
5:   for  $(u, v)$  in  $\text{lower\_star}(v)$  do
6:     Assert  $u \in T$ 
6:     if  $cc(u) = cc(v)$  then
6:       Edge_tag( $u, v$ ) = loop edge
6:       Continue
7:     else
7:       Edge_tag( $u, v$ ) = tree edge
7:       younger_cc =  $\arg \max_{w=cc(u), cc(v)} f(w)$ 
7:       older_cc =  $\arg \min_{w=cc(u), cc(v)} f(w)$ 
7:        $pers = t - f(\text{younger\_cc})$ 
8:       if  $pers \geq \theta$  then
8:         Edge_tag( $u, v$ ) = watershed edge
8:         Continue
9:       end if
10:      for  $w$  in younger_cc do
10:         $cc(w) = \text{older\_cc}$ 
11:      end for
11:       $PD = PD + (f(\text{younger\_cc}), t)$ 
12:    end if
13:  end for
14: end for
15: return Membrane_vertex_set =  $\cup$  vertices of watershed_edge_set
```

The posterior net randomly draw samples from posterior distribution $\epsilon \sim N(\mu_{post}, \sigma_{post})$. To implement the posterior net as a neural network, we will need to backpropagate through random sampling. The issue is that backpropagation cannot flow through random node; to overcome this obstacle, we adopt the reparameterization technique proposed in [23].

Assuming the posterior is normally distributed, we can approximate it with another normal distribution. We approximate ϵ with normally distribution Z ($Z \sim N(0, \mathbf{I})$).

$$\epsilon \sim N(\mu, \sigma), \quad \epsilon = \mu + \sigma Z. \quad (5)$$

Now instead of saying that ϵ is sampled from $Q(X, Y; \omega_{post})$, we can say ϵ is a function that takes parameter $(Z, (\mu, \sigma))$ and these μ, σ come from deep neural network. Therefore all we need is partial derivatives w.r.t. μ, σ and Z is irrelevant for taking derivatives for backpropagation.

G Datasets

Both volume and vessel datasets are used to validate the efficacy of the proposed method, and the details of the datasets are as follows:

1. *ISBI13* (volume): ISBI13 [1] is a EM dataset, containing 100 images with resolution of 1024x1024.
2. *CREMI* (volume): CREMI is another EM dataset, containing 125 images, and each of them has a resolution of 1250x1250.

3. *DRIVE* (vessel): DRIVE [35] is a retinal vessel dataset with 40 images. The resolution for each image is 584x565.

We use a 3-fold cross-validation for all the methods to report the numbers over the validation set.

H Evaluation metrics

The details of the metrics used in this paper are listed as follows:

1. *DICE*: DICE score is usually to measure the volumetric overlap between the predicted and ground truth masks.
2. *Adapted Rand Index (ARI)*: ARI is the maximal F-score of the foreground-restricted Rand index [29], a measure of similarity between two clusters.
3. *VOI* [20]: VOI is a measure of the distance between two clusterings.
4. *Betti Error* [17]: Betti Error measures the topology difference between the predicted and the ground truth mask. We randomly sample patches over the predicted segmentation and compute the average absolute error between their Betti numbers and the corresponding ground truth patches.

I Baselines

We compare the proposed method with two kinds of baselines: 1) Standard segmentation baselines:

1. DIVE [13] is originally designed for EM data segmentation.
2. UNet [31] achieves good performances in different contexts with encoder-decoder scheme and skip connections.
3. UNet-VGG [28] proposes a topology-aware loss based on the detected linear structures with pretrained filters.
4. TopoLoss [17] identifies the topological critical points with persistence homology and derives a novel topological loss.
5. DMT [18] identifies the whole topological structures and introduces additional penalty on the whole structures instead of isolated critical points.

2) Probabilistic-based segmentation methods:

1. Dropout UNet [21] dropouts the three inner-most encoder and decoder blocks with a probability of 0.5 during both the training and inference.
2. Probabilistic-UNet [24] introduces a probabilistic segmentation method by combining UNet with a VAE.

For all methods, we generate binary segmentations by thresholding the predicted likelihood maps at 0.5.

J Computational resources

All the experiments are performed on a RTX A5000 GPU (24G Memory), and AMD EPYC 7542 32-Core Processor.